processes

MDPI

Article

Geological Controls on Gas Content of Deep Coal Reservoir in the Jiaxian Area, Ordos Basin, China

Shaobo Xu [1,2], Qian Li [3,*], Fengrui Sun [1,2,*], Tingting Yin [4], Chao Yang [1,2], Zihao Wang [1,2], Feng Qiu [1,2], Keyu Zhou [1,2] and Jiaming Chen [1]

[1] School of Energy Resources, China University of Geosciences, Beijing 100083, China; 2106220042@email.cugb.edu.cn (S.X.)
[2] Coal Reservoir Laboratory of National Engineering Research Center of CBM Development & Utilization, China University of Geosciences, Beijing 100083, China
[3] SINOPEC Petroleum Exploration and Production Research Institute, Beijing 102206, China
[4] College of Earth Science and Engineering, Shandong University of Science and Technology, Qingdao 266590, China
* Correspondence: liqian2022.syky@sinopec.com (Q.L.); sunfengrui@cugb.edu.cn (F.S.)

Abstract: Deep coalbed methane (DCBM) reservoirs hold exceptional potential for diversifying energy sources. The Ordos Basin has attracted much attention due to its enormous resource reserves of DCBM. This work focuses on the Jiaxian area of the Ordos basin, and the multi-factor quantitative evaluation method on the sealing of cap rocks is established. The abundant geologic and reservoir information is synthesized to explore variable factors affecting the gas content. Results indicate that the sealing capacity of the coal seam roof in the Jiaxian area, with a mean sealing index of 3.12, surpasses the floor's sealing capacity by 13.87%, which averages 2.74. The sealing of the coal seam roof has a more positive impact on the enrichment of coalbed methane (CBM). In addition, the conditions for preserving gas would be boosted as coal seam thickness increased, leading to enhanced gas content in coal seams. The CH_4 content increases by an average of ~2.38 m^3/t as coal seam thickness increases with the interval of 1 m. The increasing burial depth represents the incremental maturity of organic matter and the gas generation ability in coal seams, which contributes to improving the gas content in coal seams. There is a positive correlation between the degree of coal fragmentation and the gas content of the coal seam to a certain extent. These findings provide valuable insights for targeted drilling strategies and enhancing natural gas production capacity in the Jiaxian area of the Ordos Basin.

Keywords: deep coalbed methane; Ordos Basin; gas content; cap rock sealing ability

check for updates

Citation: Xu, S.; Li, Q.; Sun, F.; Yin, T.; Yang, C.; Wang, Z.; Qiu, F.; Zhou, K.; Chen, J. Geological Controls on Gas Content of Deep Coal Reservoir in the Jiaxian Area, Ordos Basin, China. *Processes* **2024**, *12*, 1269. https://doi.org/10.3390/pr12061269

Academic Editor: Raymond Cecil Everson

Received: 29 May 2024
Revised: 14 June 2024
Accepted: 17 June 2024
Published: 20 June 2024

Copyright: © 2024 by the authors. Licensee MDPI, Basel, Switzerland. This article is an open access article distributed under the terms and conditions of the Creative Commons Attribution (CC BY) license (https://creativecommons.org/licenses/by/4.0/).

1. Introduction

Coalbed methane (CBM) plays a pivotal role in shaping the contemporary energy landscape due to its significance in diversifying energy sources and mitigating environmental impacts associated with traditional fossil fuels [1–3]. The exploration of deep coalbed methane (DCBM) resources, particularly those found at depths exceeding 1500 m, represents a frontier with immense potential for addressing energy demands sustainably. The geological reserves of CBM with depths of 1500–3000 m in China amount to approximately 30.37×10^{12} m^3 [4].

Deep coal seams are characterized by high in situ stress, temperatures, and reservoir pressure [5]. Due to the interplay of complex geological conditions, the properties of the coal seam medium, the phase state of methane storage, enhancement techniques for reservoir recovery, and the principles of fluid production differ significantly from those associated with shallow coal seams [1,2]. Recent research efforts have extensively explored the mechanisms underlying the enrichment and storage of CBM in deep coal seams. Influenced by tectonic evolution and varying preservation conditions, DCBM

systems are classified into oversaturated dry coal systems, saturated to near-saturated wet coal systems, and undersaturated wet coal systems [6]. Accordingly, it is imperative to implement development strategies that are specifically tailored to the characteristics of each type of gas-bearing system [6]. Scholars have elucidated the influence of depth on the storage states and fracturing of DCBM seams [3,7–10]. And comprehensive studies have been conducted to evaluate favorable regions [11,12]. DCBM exhibits a distinct enrichment pattern characterized by slight overpressure and high saturation adsorption storage [1]. Wide anticlines and gentle monoclines are favorable exploration areas.

The Ordos Basin, renowned for its extensive coal reserves, has emerged as a significant hub for CBM production. In 2021, the large-scale fracturing technology used in the deep eastern edge of the Ordos Basin attracted industry attention, with a gas production exceeding 10×10^4 m^3/d [13]. However, the deep strata of the Ordos Basin are characterized by a wide distribution, large thickness, and strong cyclicity of coal measures. There are rich lithological combinations and diverse reservoir formation patterns [14,15]. Significant differences exist in the enrichment laws and exploration potential of DCBM fields in various locations [16,17]. The sustained boost in production of DCBM requires a more comprehensive and in-depth study of the Ordos Basin. In the past, scholars mainly focused on the eastern edge of the basin [11]. Wei et al. [10] revealed the influence of geological conditions on the gas content and geochemistry of DCBM reservoirs in the Panji area. Chen et al. [15] optimized the key geological parameters and established a feasibility evaluation system for DCBM development in the Linxing area. Wang et al. [14] quantitatively evaluated the micro-pore and fracture structure of deep coal seams in the Daning area. However, there is currently limited research on DCBM in the central East Ordos Basin. Thus, this work would assemble large and diverse databases on the geology and reservoir performance of the No. 5 coal seam in the central East Ordos Basin. And this study uniquely explores deep coalbed methane (DCBM) resources beyond 1500 m depth, employing an integrated multifactor evaluation approach to address the limitations of previous research that focused predominantly on shallow CBM, thus providing a more comprehensive understanding of deep methane reservoirs. First is a mini-review of the geologic framework of the central East Ordos Basin. Next, we continue with the inversion models of gas content and coal structures. Then, we establish the multi-factor quantitative evaluation method on the sealing of cap rocks. Finally, this paper concludes with a discussion of the effect of geologic factors on gas content. Given the escalating demand for sustainable energy sources and the technical challenges posed by deep coal seams with their high in situ stress and temperatures, this study provides timely insights that are crucial for developing efficient extraction methods for DCBM.

2. Geologic Framework

The Ordos Basin is a large sedimentary basin in northern China. It primarily distributes in the central and western parts of the Inner Mongolia Autonomous Region, as well as parts of Shaanxi, Gansu, Ningxia, and Shanxi provinces. The formation of the Ordos Basin has undergone a long geological history dating back to the Paleozoic era. Throughout various geological periods, the basin experienced extensive sedimentation and tectonic movements, resulting in the development of rich stratigraphic sequences [18]. It features a complex depositional environment, including continental, fluvial, and lacustrine deposits. This diverse depositional environment has facilitated the formation of resources such as coal, oil, and natural gas [19]. The Ordos Basin is one of the largest coal production bases and the second-largest gas-bearing basin in China, with abundant energy resources. Currently, the development of natural gas in the Ordos Basin is a key national project.

This study focuses on the Jiaxian area in the central-eastern region of the Ordos Basin (Figure 1). The Jiaxian area within the Ordos Basin, notable for its unique Yishan Slope structural features, presents a diverse geological setting that influences coal seam distribution and gas content, forming the focal point of this study. The strata of the Ordos Basin exhibit a trend of being higher in the east and lower in the west. Multiple coal-bearing

formations have been developed within the basin from top to bottom (Figure 2). During the early Permian period of the Shanxi Formation, the Ordos Basin experienced a critical transformation from marine to terrestrial environments, marking the withdrawal of seawater from the basin and forming a typical coal-bearing sequence [20]. As depicted in Figure 2, the Shanxi Formation exhibits deltaic deposits transitioning between marine and terrestrial environments, influencing the coal seam development critical to our study's analysis of gas content. The Shanxi Formation within the basin is primarily characterized by deltaic deposits in a transitional marine-terrestrial environment. The corresponding sedimentary microfacies include distributary channel deposits, interdistributary bay deposits, swamp deposits, mouth bar deposits, and distal bar deposits. The main rock types are composed of the conglomeratic coarse sandstone, coarse sandstone, medium sandstone, fine sandstone, siltstone, and coal. Based on core observations, it can be concluded that the Shanxi Formation strata in the study area primarily consist of mudstone, sandstone, argillaceous sandstone, and arenaceous mudstone [21].

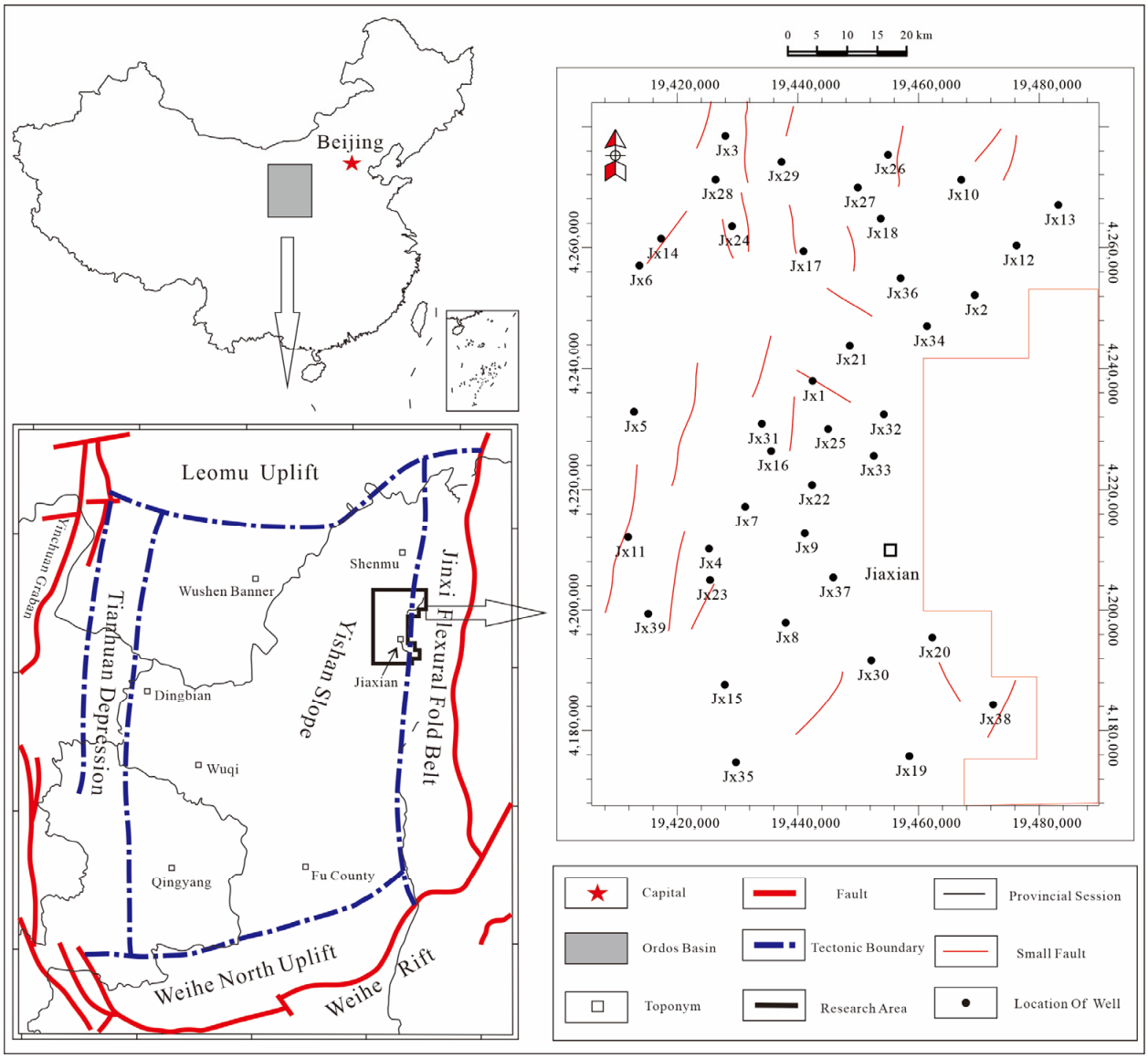


Figure 1. Location and geological structure map of the Ordos Basin study area.

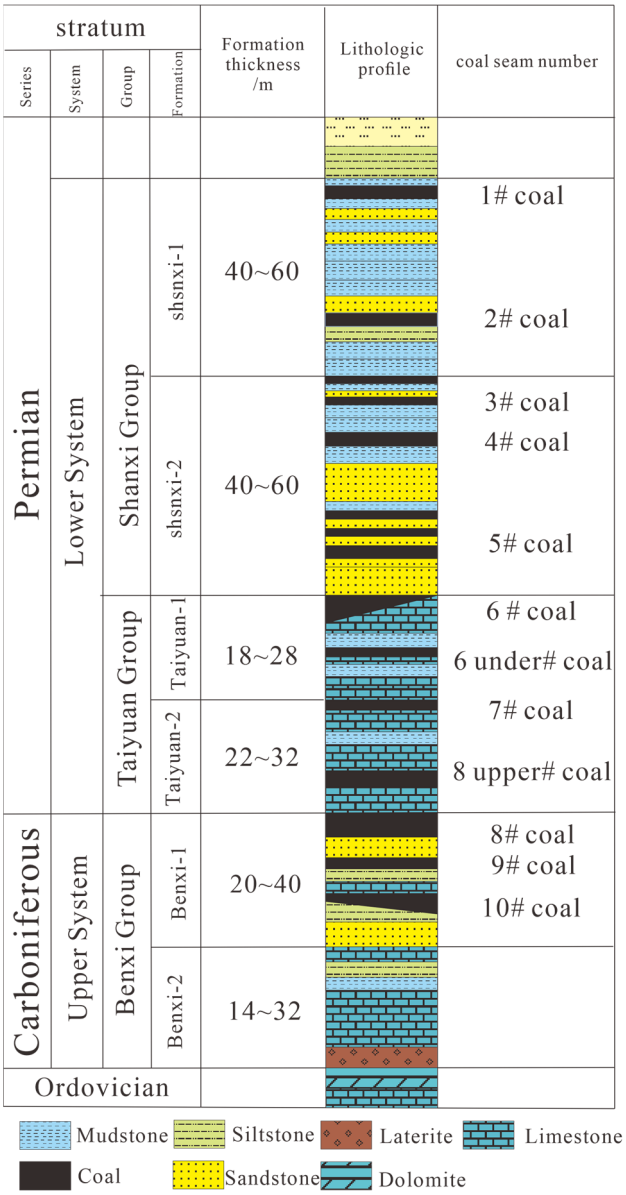


Figure 2. Lithostratigraphic column of Carboniferous–Permian strata in the Ordos Basin.

3. Inversion Models

In this study, the logging curves and interpretation data for 39 wells within the research area were collected. The coal samples were obtained for vitrinite reflectance experiments. The gas content data from the pressurized core samples were collected from 5 wells. Core observations were conducted on selected cored wells to record the results, including the macro-structure of the coal body, rock types, and rock fracture development. Additionally, breakthrough pressure experiments were performed on the mudstone and sandstone samples. Based on the logging curve data, statistical analyses were conducted on coal thickness, burial depth, and rock clay content in the coal seams.

3.1. Inversion Model of Gas Content

The No. 5 coal seam within the Shanxi Formation in the study area is stably distributed. In the absence of gas content data, it could be possible to estimate gas content across the entire area based on the logging curves. Due to the lack of measured gas content data for the No. 5 coal seam, an empirical equation for logging inversion of gas content was derived based on the measured gas content data from the nearby No. 8 coal seam in the same study

area. Pearson correlation analysis was conducted between the measured gas content data from five wells in the No. 8 coal seam and the logging curves.

The Pearson correlation coefficient analysis revealed that the DEN, GR, RLLD, and RLLS logging curves showed a good correlation with the gas content in coal seams. Based on the correlation analysis and the petrophysical properties of coals, the logging response characteristics of gas content in coal seams are as follows:

There is a negative correlation between the values of density log and gas content. The values of density response increase with the degree of coal seam compaction. Coal has the characteristic of having a lower density compared to other rocks. The CBM is mainly adsorbed within the coal seams. The richer the coal seam pores, the lower the compaction degree, and the higher the adsorbed gas content, resulting in lower coal density.

There is a negative correlation between the values of natural gamma and gas content. The coal matrix generally displays low radioactivity. When the clay minerals in coal increase, the values of natural gamma exhibit relatively high anomalies. However, the adsorption capacity of the coal seam decreases correspondingly, leading to a reduction in gas content as a result.

There is a positive correlation between resistivity and gas content. CBM is a non-conductive medium, causing an increase in coal seam resistivity. The more abundant the coal seam pores, the higher the gas content, and the greater the resistivity. Therefore, the gas content in coal seams is positively correlated with the resistivity log response.

Based on these four logging curves and the related measured gas content data, a logging response inversion model for gas content was established by Equation (1):

$$GAS = -21.48DEN - 0.022GR - 1.48Lg(RLLD) + 3.94Lg(RLLS) + 41.59 \quad (1)$$

$$R^2 = 0.74$$

Based on the data, an empirical Equation (1) for logging inversion of the gas content in coal seams was derived. The predicted gas content was obtained by using the logging inversion formula and compared with the measured gas content. The inversion model showed a high accuracy with a Pearson correlation coefficient of 0.7425 between the predicted and measured gas content, indicating a robust predictive capability (see Figure 3). In addition, the developed logging response inversion model for gas content was validated with additional measured data from adjacent wells, demonstrating a prediction accuracy within a 2–6.21% error range, as shown in Table 1.

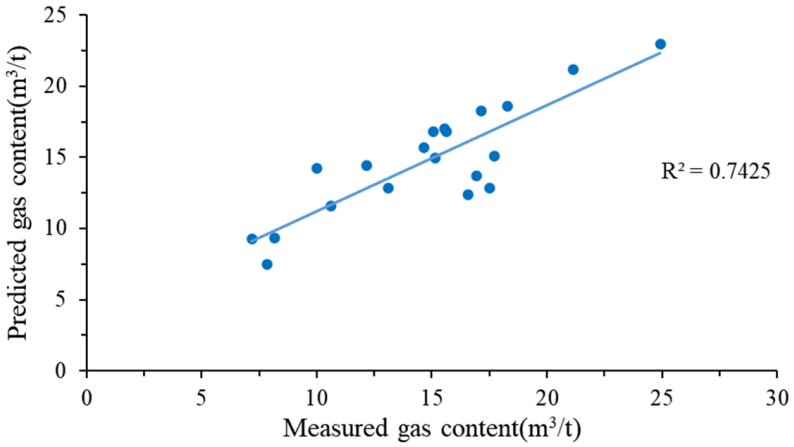


Figure 3. Relationship between measured and predicted gas content.

The existing Equation (1) was then used to predict gas content for all individual wells in the study area (Figure 4).

Table 1. Difference between measured gas content and predicted gas content in validated well samples.

Sample No.	Lithology	Measured Gas Content (m^3/t)	Predicted Gas Content (m^3/t)	Gas Content Error (%)
1	Coal	24.80	23.25	6.21%
2	Coal	23.24	23.71	2.03%
3	Coal	23.65	23.00	2.73%

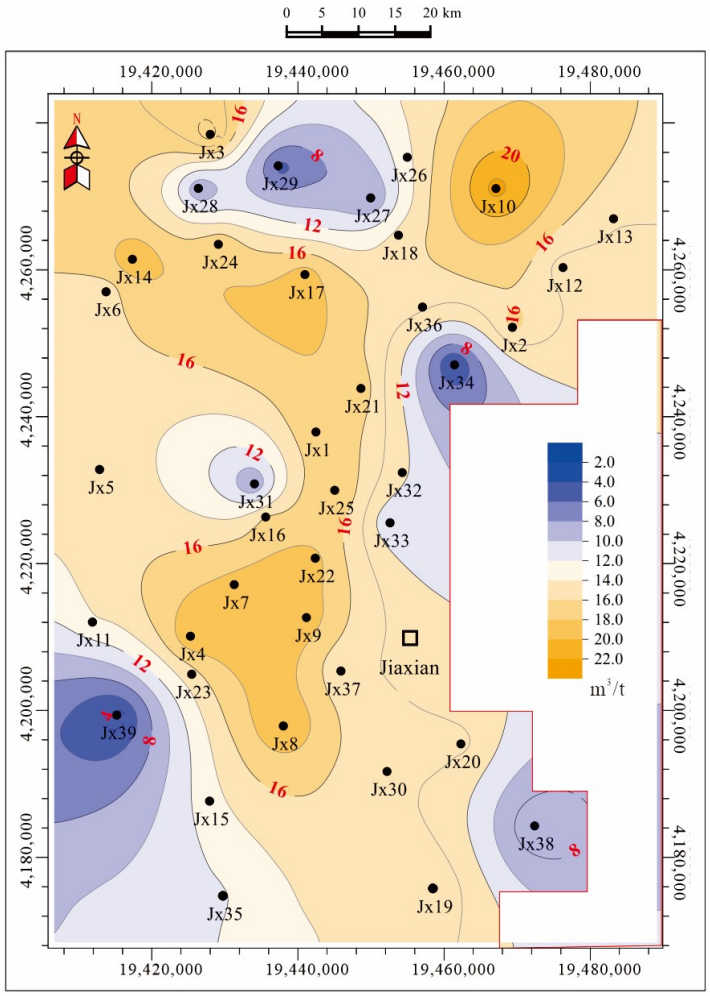


Figure 4. Map for predicted gas content of No. 5 coal seam in the Shanxi formation.

3.2. Inversion Model of Coal Structures

The logging data have been demonstrated with high accuracy in inverting coal body structure and macroscopic coal rock types. The coal body structure reflects the variations in the degree of fragmentation and differences in easily evolving coal body structures of different coal rock types. It is manifested in the logging interpretation as changes in acoustic transit time (AC), resistivity (RLLD, RLLS), density (DEN), and natural gamma (GR) [22]. By combining the well-controlled logging data within the study region, the development characteristics of deep coal body structures in the basin were analyzed [23].

Since the mylonitic structures are less developed and often coexist with granulated structures in the study area, the coal body structure was classified into three categories: Primary, fractured, and granulated/mylonitic. Based on Pearson correlation coefficients, an analysis was conducted to establish the correlation between the complete set of logging curves and the coal body structure, considering coefficients greater than 0.2 as indicative of a significant correlation.

The logging curves with good correlation were used as inversion parameters, including AC, CNL, DEN, GR, RLLD, RLLS, and RT. Due to compression and shearing effects, tectonic coal has increased internal fractures and pores, resulting in slower acoustic wave propagation and consequently higher AC values. Tectonic coal has higher porosity and possibly higher water saturation; thus, the porosity indicated by the CNL log curve increases. Due to fracturing and the development of cracks, the overall density of tectonic coal decreases, leading to lower DEN values. The GR value of coal seams is usually low, but if tectonic coal contains clay or other materials with higher radioactivity, the GR value may increase. With increased porosity and fractures, the water content of tectonic coal also increases, resulting in lower resistivity, thus reducing RDDL and RDDS values. The RT of tectonic coal is generally lower due to its high porosity and water content. Therefore, these logging parameters are selected as inversion parameters for coal structure analysis.

The logging curve data were first preprocessed, including two main steps: Data standardization and outlier removal. Data were standardized to a range of 0–100. The outliers were removed based on the principle of exceeding three standard deviations from the normal distribution. After processing, the normalized data were used for the original treatment. Coal samples were utilized to develop a logging inversion model for the coal body structure by Equation (2).

$$y = 0.0003AC - 0.0393CAL - 0.0618DEN - 0.0024GR + 1.2173Lg(RD) + 0.3466Lg(RS) - 1.1967Lg(RT) + 1.457 \quad (2)$$

The fitting criteria for the coal body structure were defined as follows: y $\leq$ 0.5 indicates a primary structure; 0.5 < y $\leq$ 1 indicates a fractured structure; y > 1 indicates granulated and mylonitic structures. It turned out that the prediction accuracy of the coal body structure reached 81%. The equation was subsequently applied to the No. 5 coal seam in the study area. To facilitate the exploration of the relationship between coal body structure and gas content, the Coal Fracture Index (CFI) was introduced. It was calculated for individual wells based on different degrees of coal body damage by Equation (3), with parameters increasing sequentially with the degree of coal body damage.

$$CFI = \sum_{i}^{3} A_i H_i \quad (3)$$

where H_i is the thickness of coal with different coal body structures; A_i is the parameter of coal seam damage degree, set them to 0.25, 0.5, and 0.87, respectively.

4. Evaluation of Cap Rock Sealing Ability

4.1. Classification of Cap Rock Lithology

Identifying the lithology of cap rocks is fundamental to studying cap rock sealing properties. Based on the investigation of the depositional environment and core observations within the study area, it was determined that the primary lithologies of the coal seam cap rocks include mudstone, sandstone, argillaceous sandstone, and arenaceous mudstone. Due to the insufficient core observation data, only the roof and floor lithology of the coal seam in a few wells could be determined. Since the cap rocks are mostly mudstone and sandstone, the logging curves include three mudstone content curves (SH) and a sandstone content curve (SAND). Therefore, it is proposed to use the shale content curve (SH) to identify the lithology of the coal seam roofs and floors in this study. The classification is as follows: Rocks with shale content greater than 75% are classified as mudstone; rocks with shale content greater than 50% and less than 75% are classified as arenaceous mudstone; rocks with shale content greater than 25% and less than 50% are classified as argillaceous sandstone; rocks with shale content less than 25% are classified as sandstone. Using this logging-based lithology classification method, the lithology of the coal seam roofs and floors was determined for 39 wells in the study area (Figure 5).

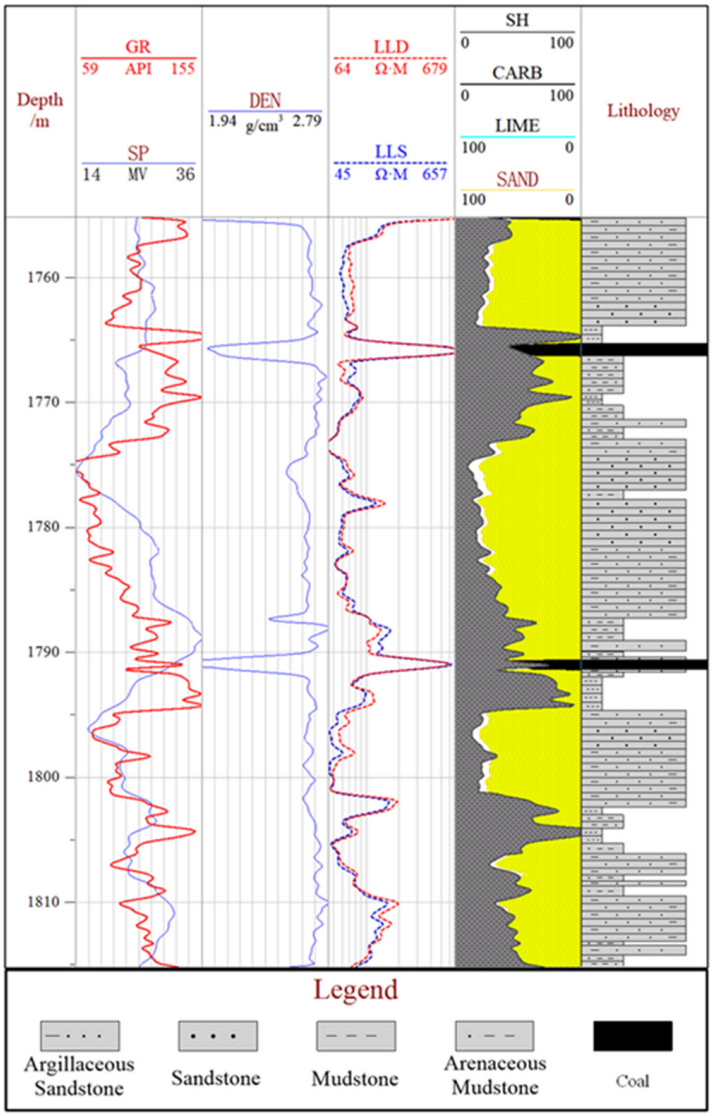


Figure 5. Column diagram of lithology division of Jx5 well.

4.2. Fracture Developent

In this study, the sealing capacity of the coal seam roofs and floors is explored from four aspects: Shale content, layer thickness, breakthrough pressure, and fracture development index. The impact of these geological parameters on the calculation of seal integrity and the determination of parameter values will be discussed subsequently.

Generally, different lithologies have the varying sealing capacities for oil and gas. Previous research has shown that the sealing capacity of mudstone, limestone, and sandstone gradually decreases. For a given thickness, mudstone's CBM sealing capacity is nearly 17 times higher than that of sandstone [24]. The target coal seams are located in the middle part of the Shan 2 member of the Shanxi Formation. The upper and lower lithological layers of the coal seam consist of interbedded mudstone and sandstone. Therefore, under the condition of considering only two types of lithology, the mud content is considered to be a key factor when evaluating the sealing capacity of the cap rocks in a coal reservoir. Based on the logging curves of mudstone and sandstone content, the cap rocks are classified into mudstone, sandstone, argillaceous sandstone, and Arenaceous mudstone. The higher the average shale content in a single lithologic layer, the better its sealing performance. The mudstone quality of a single lithologic layer can be calculated using the GR logging curve.

When determining the seal integrity of the top and bottom cap layers, we stratify the lithology within a certain thickness range of the coal seam top or bottom, dividing it into

the aforementioned four types of rock. For the evaluation of the sealing performance of individual wells, the thickness of each layer must also be considered in addition to the lithological classification. The thickness of a single rock layer is a critical indicator of its macroscopic extent. The greater the thickness of a single rock layer, the more stable the depositional environment and the lower the likelihood of structural alteration [25]. The less connected the micro-leakage pathways in the rock, the lower the gas migration rate, allowing for the accumulation and preservation of oil and gas over long geological periods. Therefore, single-layer thickness is used as an evaluation criterion in the sealing capacity assessment model. The thicker lithologic layers provide better sealing conditions for oil and gas.

Breakthrough pressure is an essential measure of the cap rock's capillary sealing. The breakthrough pressures of selected rock samples are determined using the displacement method, which relies on capillary pressure. The process begins by saturating the rock sample with a wetting fluid, after which a non-wetting fluid is injected to displace the wetting fluid, overcoming the rock's capillary forces. Before the experiment, the rock sample is saturated with formation water and placed under a specific confining pressure. Gas is then injected into one end of the core, and the injection pressure is gradually increased and maintained. The pressure at which the gas breaks through and escapes from the opposite end of the core is recorded as the breakthrough pressure of the rock. Due to a large number of wells but limited samples, experiments focused only on the breakthrough pressures of the roof and floor rocks of coal seams from a single gas well. Consequently, scholars suggested using geophysical logging to predict breakthrough pressures for these rocks in wells without core samples [26]. By fitting experimental pressure data with acoustic transit time, a formula was developed to calculate breakthrough pressures for all wells in the area based on acoustic travel time logging curves for the roof and floor rocks of each well.

The propagation speed of acoustic waves in formations is influenced by various factors, including lithology, density, rock structure, and fluid properties. For sandstone and mudstone, the acoustic transit time is mainly affected by compaction. The compaction degree in sandstone and mudstone is primarily reflected by porosity, which has a clear linear relationship with acoustic transit time. Greater acoustic transit time indicates higher porosity, and porosity is negatively correlated with breakthrough pressure. Higher porosity means lower breakthrough pressure, making it easier for gas to pass through the rock. Thus, there is a functional relationship between acoustic transit time and breakthrough pressure [27]. The model of breakthrough pressure based on acoustic transit time is widely used for the logging interpretation of this parameter. The corresponding experiments were conducted on samples collected from the coal seam roofs and floors (shown in Table 2).

Table 2. Test results of breakthrough pressure for roof and floor rocks of the coal seam.

Serial Number	Lithology	Length /cm	Diameter /cm	Saturated Liquid	Test Gas	Confining Pressure/MPa	Breakthrough Pressure/MPa
1	Siltstone	5.05	2.45	Formation Water	Nitrogen	35.00	26.05
2	Argillaceous siltstone	5.15	2.51	Formation Water	Nitrogen	46.00	44.01
3	Carbonaceous mudston	5.11	2.46	Formation Water	Nitrogen	41.00	39.02
4	Gravelly coarse sandstone	5.03	2.52	Formation Water	Nitrogen	35.00	1.50
5	Sandstone	5.02	2.52	Formation Water	Nitrogen	35.00	0.32
6	Mudstone	5.08	2.49	Formation Water	Nitrogen	43.00	42.00
7	Mudstone	5.01	2.49	Formation Water	Nitrogen	43.00	40.20
8	Silt-bearing mudstone	5.14	2.51	Formation Water	Nitrogen	35.00	24.02

Based on the above theory, the breakthrough pressure experiments were conducted using core samples from five wells in the study area, combined with previous experimental results [27]. The experimental data of the rocks were fitted with the AC (acoustic transit time) logging curves (Figure 6). The results show that there is a negative correlation between breakthrough pressure and acoustic transit time, with a correlation coefficient of 0.80. It can be expressed with the following Equation (4):

$$P = 89471e^{-0.037\Delta t} \quad (4)$$

where P is the breakthrough pressure of the rock, MPa; Δt—the sound wave time difference of the rock, μs/m.

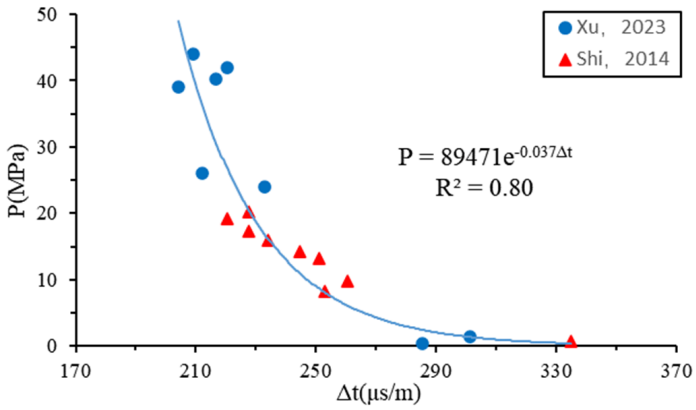


Figure 6. Relationship between rock breakthrough pressure and acoustic transit time [27].

For oil and gas reservoirs, the faults or fractures could significantly impact the sealing capacity of the fluid. It is easy to form a large number of fractures near the fault zone [28]. Fractures play a crucial role in the production and migration of oil and gas, especially in the roofs and floors of coal seams. Various direct and indirect methods are currently available to predict the degree of fracture development in formations, such as seismic analysis, petrophysical logging, well testing, core analysis, and image logging [29]. However, each method has its limitations. For example, the seismic methods can only be applied to display the information about large-scale fractures and faults. The core analysis also has significant limitations in terms of low recovery rates in fractured zones, undirectional coring, and high coring costs. Petrophysical logging is an effective method for identifying fractures. However, it is essential to note that a single type of logging cannot determine fracture zones [30]. Therefore, a combination of logging methods should be used for fracture detection [31].

Typically, conventional logging includes nine types of logging data: three porosity logs (density log (DEN), acoustic transit time log (AC), compensated neutron log (CNL)), three lithology logs (gamma ray log (GR), caliper log (CAL), spontaneous potential log (SP)), and three resistivity logs (deep resistivity log (Rt), shallow resistivity log (Rxo), and invaded zone resistivity log (RI)).

The fracture response characteristics of conventional logging curves have been extensively researched in previous studies. Generally, acoustic waves may reflect, refract, or scatter on the fracture surfaces, lengthening the propagation path and increasing the acoustic transit time. Additionally, the entry of mud components into the fractures during drilling can also increase the AC value. When drilling through fracture zones, fractures can cause the surrounding rock to collapse, enlarging the borehole and causing the CAL value to exceed the drill bit diameter. Uranium precipitation from formation water in fractures can cause an increase in the GR value [32]. Fractures in rocks increase porosity, and since fluid density is lower than rock density, fractures reduce the DEN value. The CNL measures hydrogen content in formations, and fractures slightly increase fluid content,

raising the CNL value. Fractures significantly enhance reservoir permeability and flow capacity, negatively impacting SP [33].

As such, conventional logging curves exhibit good fracture responses (Figure 7). Combining logging curve variations with core observations helps identify logging curves with good fracture responses. In well Jx1, the DEN and SP logging curves show noticeable drops at three core-observed fracture locations. This is because fluid-filled fractures in the formation have a lower density than the rock, reducing the DEN log value. The SP log value decreases in fractured areas due to changes in formation water conductivity. Fracture-pore water generally has higher conductivity than surrounding rock-pore water because fractures provide larger flow channels, facilitating water exchange. Fracture water is typically fresher, with lower salinity and higher conductivity. When high-conductivity fracture water contacts high-salinity drilling mud, the natural potential difference is smaller than in areas with fewer or no fractures, resulting in lower SP log values in fractured zones [34,35].

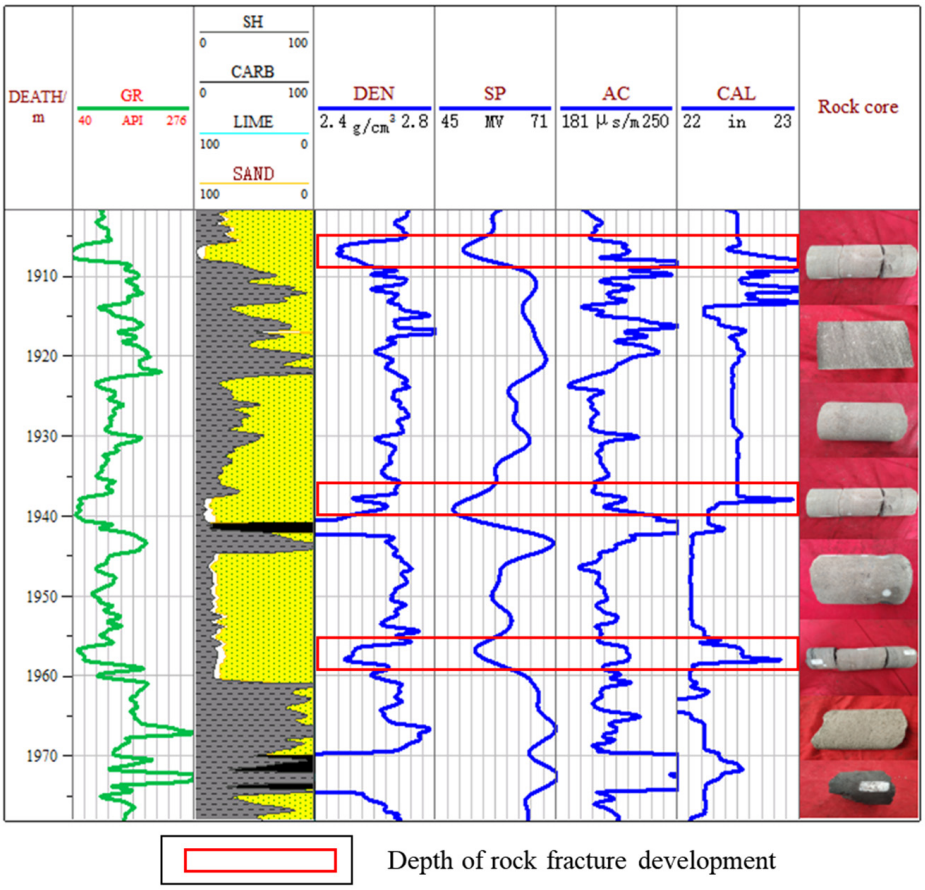


Figure 7. Fracture-related logging curve responses for Well Jx1.

Conversely, the AC and CAL log values increase. The AC log value increases because fractures disrupt rock continuity, reducing the effective elastic modulus [36]. When fractures are present, the reduced elastic modulus slows acoustic wave velocity, increasing the AC log value. Additionally, in heavily fractured formations, acoustic waves may bypass fractures or travel complex paths, lengthening the propagation path and increasing the AC log value. The CAL log value increases because fractures weaken the overall rock structure, making the borehole wall more prone to collapse or break during drilling. This is especially evident when the borehole passes through fractured formations, as fractures provide weak points that make the rock more susceptible to damage during drilling, increasing the CAL log value [37,38].

Based on the comparison between logging responses and fractures observed in core samples, the DEN, SP, AC, and CAL logging curves were selected as fracture development response curves. Since the presence of fractures in the formation causes anomalous changes in the logging curves, we introduced the anomalous change response index (ACRI). When fractures are present, the ACRI is calculated using different equations depending on whether the logging values decrease or increase.

For logging curves where values decrease (such as DEN and SP), the ACRI is calculated using Equation (5):

$$ACRI = \frac{A_{\max} - A_t}{A_{\max} - A_{\min}} \quad (5)$$

For logging curves where values increase (such as AC and CAL), the ACRI is calculated using Equation (6):

$$ACRI = \frac{A_t - A_{\min}}{A_{\max} - A_{\min}} \quad (6)$$

where A_t is well log curve values corresponding to the target layer; $A_{\max}$ is the maximum values corresponding to individual well log curves; $A_{\min}$ is the minimum values corresponding to individual well log curves.

Since the degree of fracture development cannot be determined using a single logging curve alone, multiple logging curves need to be considered. The fracture identification index (FFI) is calculated by assigning appropriate weights to the anomalous change response indices (ACRI) from each logging curve. The weighted combination of these indices provides a comprehensive measure of fracture development. FFI is calculated by Equation (7):

$$FFI = \sum_{i=1}^{n} m_i ACRI_i \quad (7)$$

In the equation: n—the number of abnormal change response indices. n = 4; m_i—the weight coefficients of the abnormal change response indices, based on the sensitivity of the four fracture-sensitive curves DEN, SP, AC, CAL, are, respectively, taken as 0.15, 0.25, 0.35, 0.25; $ACRI_i$—the abnormal change response indices corresponding to each curve.

4.3. Cap Rock Thickness

The sealing capacity of the coal seam roofs and floors depends not only on the physical properties of individual rock layers but also on the overall thickness of the roofs and floors. Thickness is a crucial parameter affecting the cap rock's ability to seal natural gas. It influences the spatial extent of the cap rock and, to some extent, its sealing quality. For the same set of coal seams, the greater the thickness of the cap rock, the larger its spatial extent, which is more favorable for hydrocarbon accumulation. Conversely, thinner cap rocks have a smaller spatial extent and weaker natural gas sealing capacity, making them less favorable for gas accumulation and preservation.

The Ordos Basin currently includes several gas fields under exploration and development, such as the Sulige Gas Field, Jingbian Gas Field, and Changdong Gas Field. Their main gas-producing formations are all from the Early Permian strata, with cap rock thicknesses of 20 m, 27.5 m, and 20 m, respectively [39]. On the other hand, the statistical analysis of coal seam thickness in the study area shows that the average thickness of the No. 5 coal seam in the Shanxi Formation is 2.70 m. The coal seam is generally well-developed and stable, with minimal lithological variation in the roofs and floors of different wells (Figure 8). Compared to other coal-bearing formations, the No. 5 coal seam is relatively thin, and the roofs and floors primarily consist of mudstone and sandstone, with stable lithology development.

Therefore, the rock layers within 20 m above and below the coal seam were taken as the sealing layer for the coal seam to calculate its sealing performance.

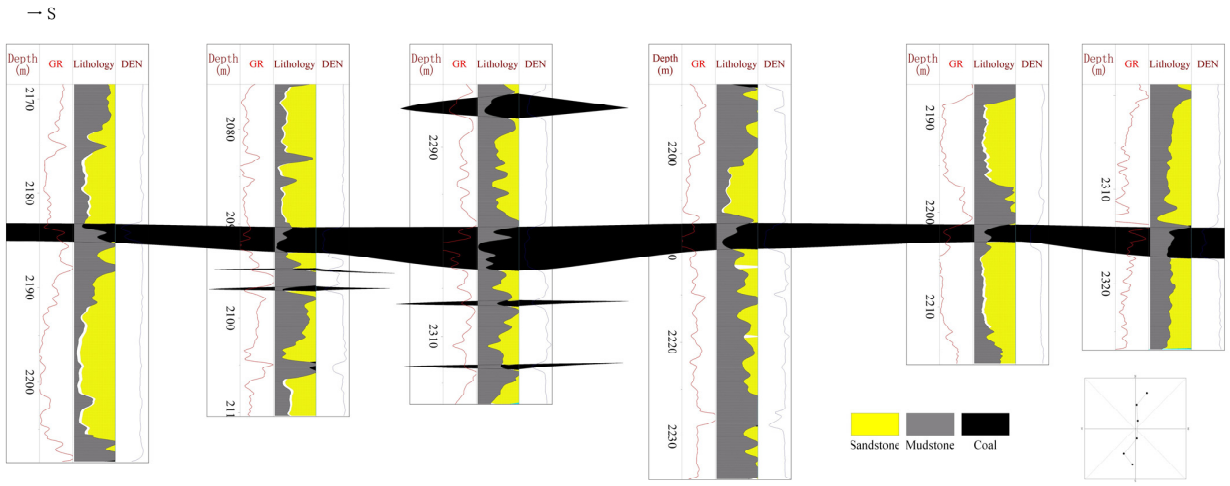


Figure 8. North-south well correlation profile of No. 5 coal seam.

4.4. Comprehensive Analysis of the Sealing Capacity of Roof and Floor Rocks

Using the existing data, logging data within 20 m above and below the coal seam were read. Depth correction of the logging curves was performed based on the existing core data. The shale content, thickness, breakthrough pressure, and fracture identification index of each rock layer were calculated using the logging data and the previously established model. The four evaluation indices for individual rock layers in each well were obtained (Table 3).

Table 3. Evaluation parameters for the sealing capacity of single rock layers in the roof and floor of No. 5 coal seam.

Well ID	Location	Rock Type	Layer Thickness	Mud Content	Breakdown Pressure	FFI
Jx13	roof	mudstone	9.50	77.08	32.14	0.33
		Arenaceous mudstone	3.00	62.05	36.25	0.38
		argillaceous sandstone	7.50	26.64	34.51	0.60
	floor	mudstone	3.625	82.86	35.95	0.22
		Arenaceous mudstone	4.125	51.81	35.65	0.27
		sandstone	10.87	23.67	34.698	0.43

Based on the above analysis, it is known that the sealing capacity of the roof and floor is positively correlated with layer thickness, shale content, and breakthrough pressure, and negatively correlated with the fracture identification index. Considering the influence mechanisms of each parameter on sealing capacity, a weighted influence method was used to assign weights to each parameter. A single-layer sealing evaluation index (SI) was introduced to construct a quantitative calculation for the sealing capacity of individual rock layers by Equation (8).

$$SI_S = AT + BV_S + CP - D \cdot FFI \quad (8)$$

In the equation: T—single-layer rock thickness, m; V_S—clay content, %; P—breakthrough pressure, MPa; A,B,C,D—the weight assigned to each parameter, dimensionless.

Based on the above rules, the weight parameters are assigned to each sealing capacity evaluation parameter such that A + B + C + D = 1. Based on the impact of each parameter on sealing capacity, sensitivity analysis was used to assign weights. The weight values (A = 0.25, B = 0.30, C = 0.25, D = 0.20) reflect their influence on sealing capacity. Firstly, in terms of sealing capacity, clay content is the most critical factor. As clay content increases, sealing capacity also increases. Thickness and breakthrough pressure are important influencing factors following clay content, with data derived from well logs and measured breakthrough pressure, ensuring accuracy. The fracture development index, entirely an-

alyzed from well log data, reflects the degree of formation fracturing to a certain extent. Parameter values were assigned based on the influence of each factor on sealing capacity.

Due to the different physical meanings, numerical ranges, and units of each evaluation parameter, it is necessary to preprocess these parameters to eliminate the dimensional effects before calculating the single-layer sealing capacity. Data processing employed a standardization method, adjusting each parameter's values to the 0–1 range based on their minimum and maximum values to ensure comparability among parameters with different ranges. This eliminates the dimensions of the parameters and allows them to be used in the calculation of the sealing index. The data standardization formula is as follows Equation (9):

$$X = \frac{X - X_{\min}}{X_{\max} - X_{\min}} \tag{9}$$

In the equation: X, $X_{\max}$, $X_{\min}$—these are the original values, maximum values, and minimum values for the parameters, respectively.

Based on the calculated data, we can determine the sealing capacity of each individual rock layer within 20 m above and below the No. 5 coal seam in the Shanxi Formation. For evaluating the overall sealing capacity of the roof and floor, it is not sufficient to simply sum the sealing evaluation indices of each layer. This approach might overlook the fact that rock layers at different distances from the coal seam contribute differently to the overall sealing capacity. Therefore, after calculating the single-layer sealing evaluation index (SIs) for each layer, it is necessary to introduce a distance influence coefficient (DIC) to balance the contribution of rock layers at varying distances from the coal seam. DIC is calculated by Equation (10):

$$DIC = \frac{20 - D}{20} \tag{10}$$

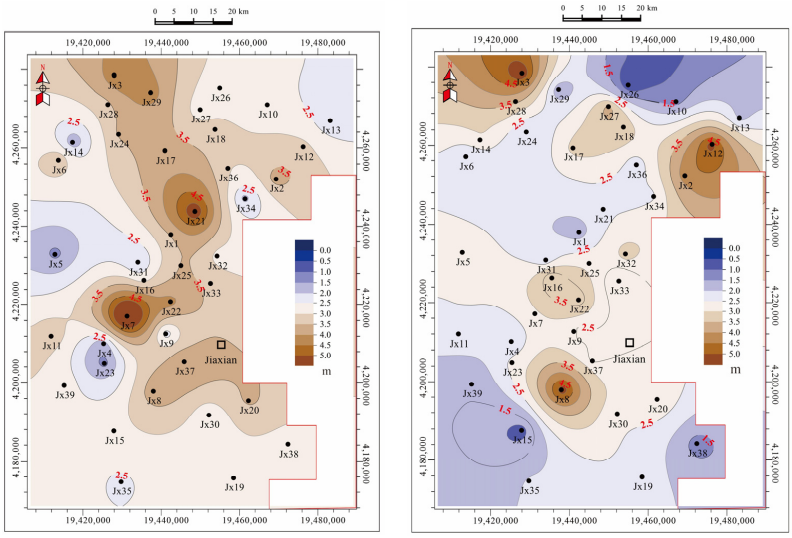
In the equation: D—distance from the target layer to the coal seam, m.

Based on the method described above, the equation for constructing the calculation model of the roof and floor sealing index is as follows Equation (11):

$$SI = \sum_{j=1}^{m} DIC_j \cdot SI_{sj} \tag{11}$$

In the equation: m—top or bottom rock lithology stratification.

By calculating the sealing capacity of the coal seam roofs and floors for each well in the study area, an isogram of the sealing capacity of the coal seam roofs and floors can be generated (Figure 9).



(**a**) (**b**)

Figure 9. Contour map of the sealability index for the roof and floor of the No. 5 coal seam. (**a**) Sealing index of coal seam roof; (**b**) sealing index of coal seam floor.

5. Geological Factors Affecting Gas Content

5.1. Effect of Cap Rock Sealing Capacity on Gas Content

Based on the above calculation results, the sealing control effects of the rock roof and floor on the gas content in coals are explored. The relevant relationships are displayed in Figure 10.

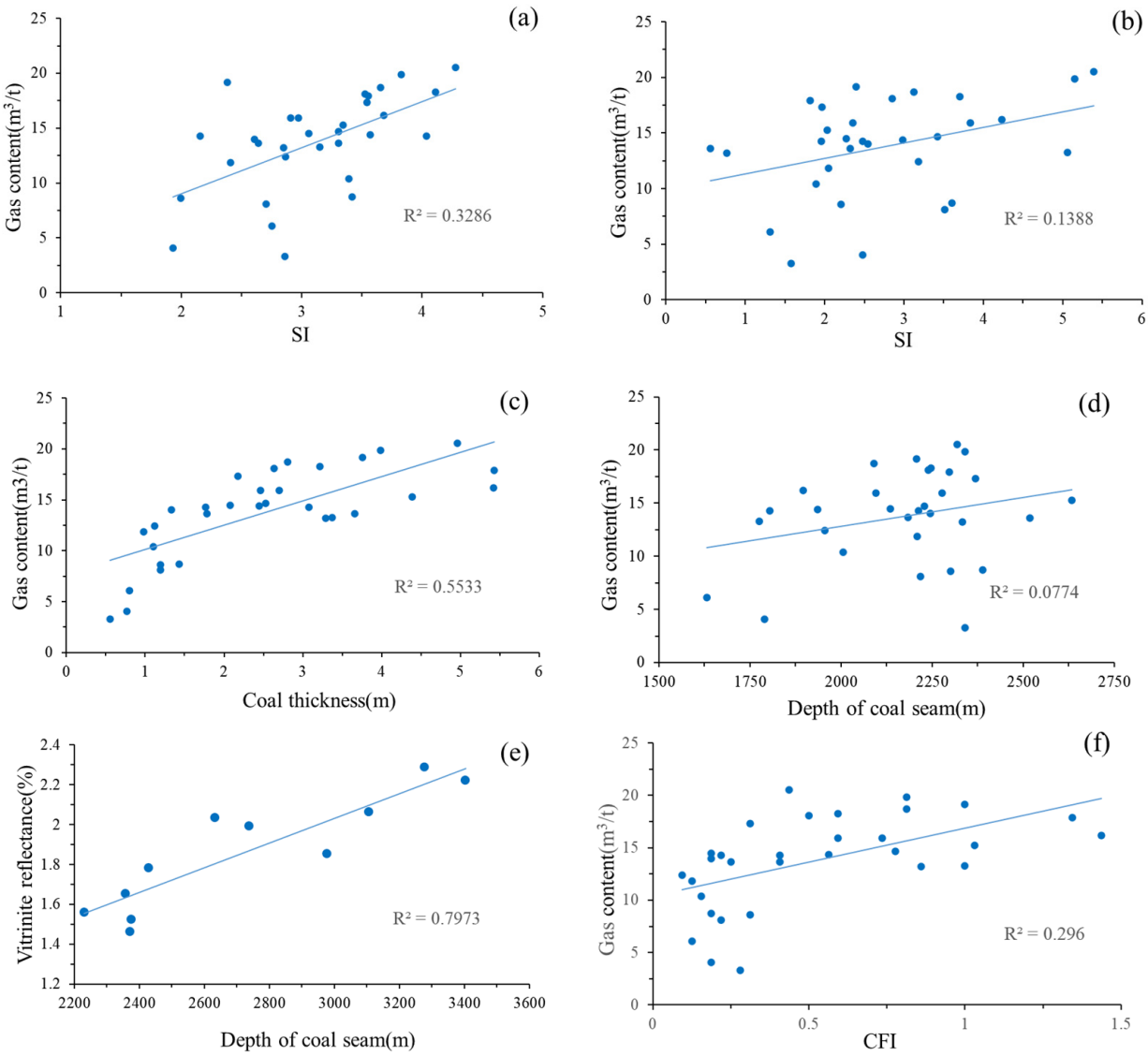


Figure 10. Relationship between ground quality control factors and gas content in No. 5 coal seam and the variation of vitrinite reflectance with buried depth. (**a**) Roof SI and gas content; (**b**) floor SI and gas content; (**c**) gas content and coal thickness; (**d**) gas content and depth of coal seam; (**e**) vitrinite reflectance and buried depth of coal seam; (**f**) gas content and coal failure index.

From Figure 10a, it can be observed that the gas content of the No. 5 coal seam increases with the improvement of the sealing integrity of the roof, showing a significant correlation. This indicates that the sealing integrity of the coal seam roof influences the gas content of the coal seam to a certain extent. From Figure 10b, it can be seen that the gas content of the No. 5 coal seam also increases with the improvement of the sealing integrity of the floor. In Figure 10a, the slope of the trend line is 4.20, while in Figure 10b, the slope of the trend line is 1.40. This shows that the increase in gas content due to improved floor sealing is much less significant than the increase due to improved roof sealing. The correlation between roof sealing integrity and gas content is 0.3286, while the correlation between floor sealing integrity

and gas content is 0.1388, indicating that the correlation between roof sealing integrity and gas content is stronger than that between floor sealing integrity and gas content. This may be because the lighter gas in the coal seam tends to migrate upwards in the formation, making the roof sealing integrity more relevant to gas content.

Therefore, the sealing capacity of the roof and floor of the coal seam affects the gas content differently, with the roof's sealing integrity having a greater impact on the gas content. The comprehensive results indicate that the sealing capacity of the coal seam roof in the Jiaxian area (average sealing capacity of 3.12) is 13.87% higher than the sealing capacity of each individual roof layer (average sealing capacity of 2.74). These findings provide valuable insights for targeted drilling strategies and increasing natural gas production in the Jiaxian area.

5.2. Effect of Coal Seam Thickness on Gas Content

The gas content of coal seams is not only related to the preservation conditions of the closure but also to the physical properties of the coal seams themselves, such as coal thickness, burial depth, and coal structure [40]. This paper investigates the relationship between coal seam thickness, burial depth, coal structure, and gas content, as well as the relationship between vitrinite reflectance and burial depth (as shown in Figure 10).

The thickness of the coal seam is another important influencing factor for the enrichment of CBM. The coal seams are both producers and reservoirs of CBM. The thickness of the No. 5 coal seam in the study area is shown in Figure 11. The thickness of the No. 5 coal seam in the study area ranges from 0.55 m to 5.43 m, with an average of 2.7 m. The overall thickness of the coal seam shows a characteristic of being thicker in the northwest and thinner in the southeast. The thickness of the coal seam varies little overall, and the coal seam development is relatively stable, with most areas having a coal seam thickness of more than 2 m. The fitting relationship between CBM content and coal thickness is illustrated in Figure 10c. As shown in Figure 10c, there is a positive correlation between CBM content and coal thickness. On the one hand, the increase in coal thickness could benefit the gas production of coals. On the other hand, the stable development of thick coal seams also enhances the gas storage capacity. The correlation coefficient is 0.5533. The reason is that the increase in coal seam thickness, on the one hand, contributes to the increase in gas production and, on the other hand, expands the gas storage space of the coal seam. Additionally, the coal seam itself can act as a sealing layer for CBM. Therefore, the increase in coal seam thickness not only enhances gas production but also improves the conditions for gas preservation, facilitating the conservation of CBM. The interaction between coal seam thickness and rock roof sealing was found to be significant, where areas with both high roof sealing (index > 4.5) and greater coal thickness (>2.5 m) exhibited the highest gas content, suggesting a synergistic effect (see Figures 9 and 11).

5.3. Effect of Coal Seam Burial Depth on Gas Content

The burial depth of the No. 5 coal seam in the study area is shown in Figure 12. The burial depth of the No. 5 coal of the Shanxi Formation is in the range of 1632.68–2658.52 m, with an average value of 2234.14 m. The burial depth of the coal seam has the characteristic of being higher in the east and lower in the west, with significant overall variations in depth. According to statistics, the burial depth of the target coal seams is mainly distributed between 1700 m and 2500 m. The burial depth as well as the gas content vary greatly in different regions within the same set of coal seams, as shown in Figure 10d. It could be seen in the figure that the gas content displays a gradually increasing trend with the depth of the coal seam.

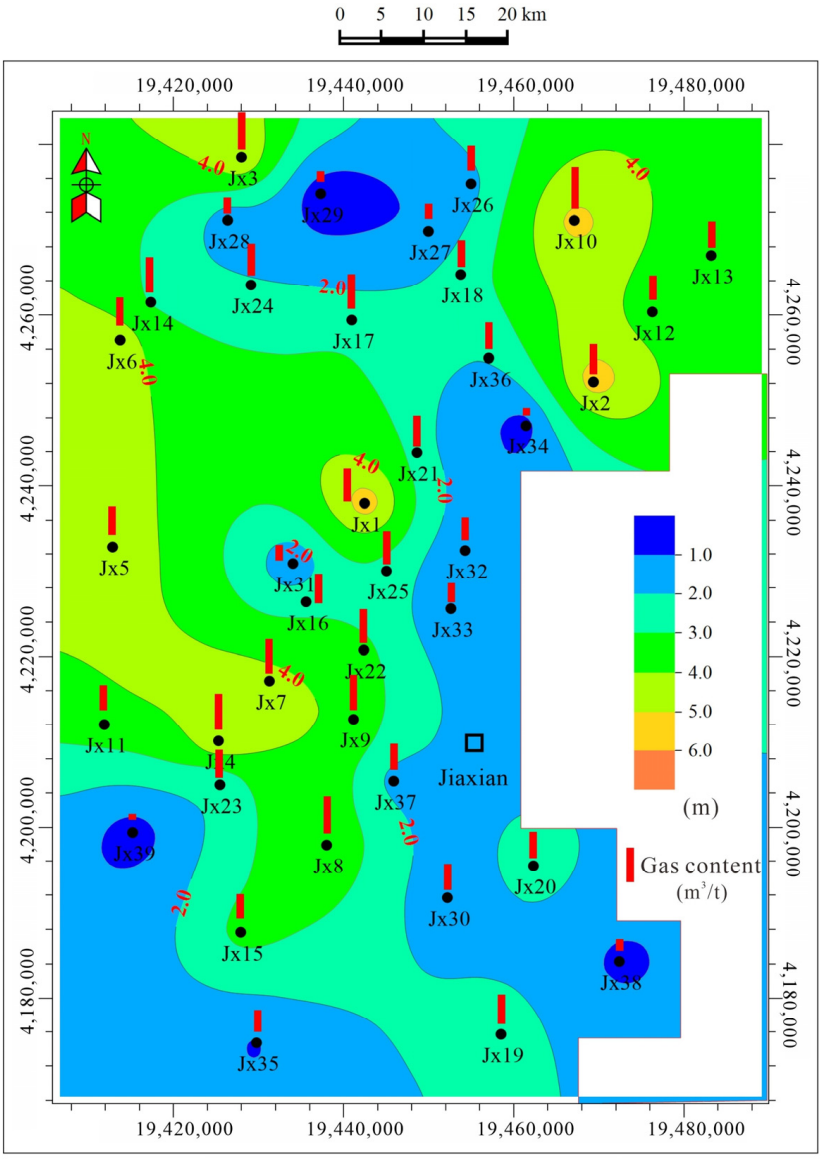


Figure 11. Contour map of No. 5 coal seam thickness.

The sources of CBM come from the coal seam itself as well as from the adjacent gas layers through diffusion. Among the parameters, vitrinite reflectance is one of the most important indicators for evaluating the gas generation potential of the coal seam itself. The vitrinite reflectance is chosen as the indicator of organic matter maturity to reflect the thermal evolution from early diagenesis to deep metamorphism. As detailed in Figure 10e, the correlation coefficient between vitrinite reflectance and burial depth is 0.7973. Burial depths of 2200–3600 m correspond to an increase in vitrinite reflectance from 1.55% to 2.29%, correlating with an enhancement in gas generation capacity. This phenomenon is attributed to the regular increase in formation temperature in deep strata. High temperatures are conducive to the maturation of organic matter, which in turn leads to an increase in the gas generation capacity of coal seams. The overall linear correlation coefficient of 0.0774 between coal seam burial depth and gas content is relatively low. This is because, although the gas generation capacity of the coal seam increases with rising vitrinite reflectance, when the vitrinite reflectance exceeds 1.5%, the porosity of the coal seam decreases, leading to a reduction in gas content. Therefore, with increasing burial depth, the gas content in the coal seam does not increase linearly but shows a trend of first increasing and then decreasing.

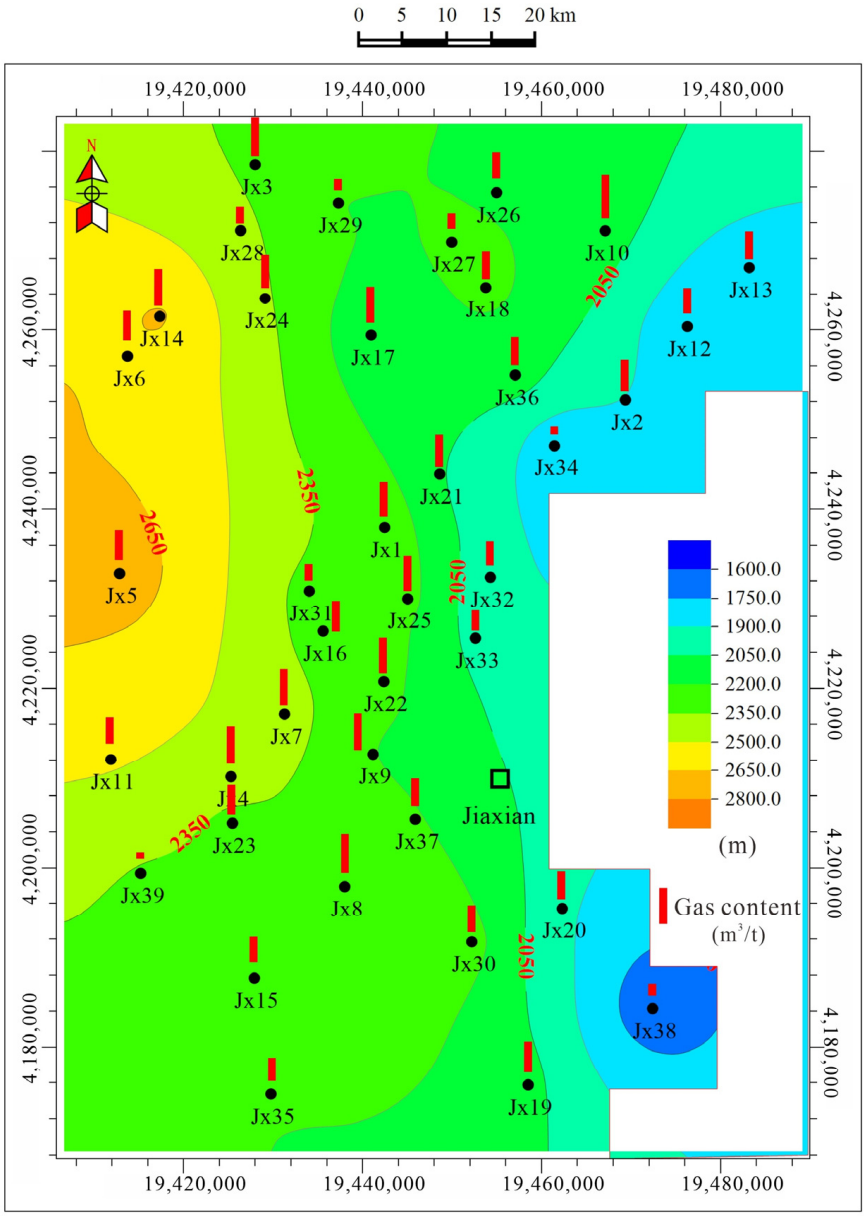


Figure 12. Contour map of No. 5 coal seam burial depth.

5.4. Effect of Coal Structure on Gas Content

The influence of tectonic action on coal seam gas enrichment has been studied [41,42], but the influence of structural change on coal seam gas content caused by tectonic action has not been discussed. On the basis of previous studies, the influence of coal structure on gas content is further discussed.

The coal body destruction index of the No. 5 coal seam in the study area is shown in Figure 13. The destruction index ranges from 0.09 to 2.00, with an average value of 0.58. The destruction index of the coal body structure is relatively high in the central and western parts of the study area, while it is lower in the southeastern region. This indicates that the coal seams in the central and western parts are more affected by tectonic activities compared to the southeastern region. The primary structure of the coal seam is destroyed, leading to the formation of more tectonic coal. Further research is conducted on the relationship between CBM content and coal failure index, as shown in Figure 10f.

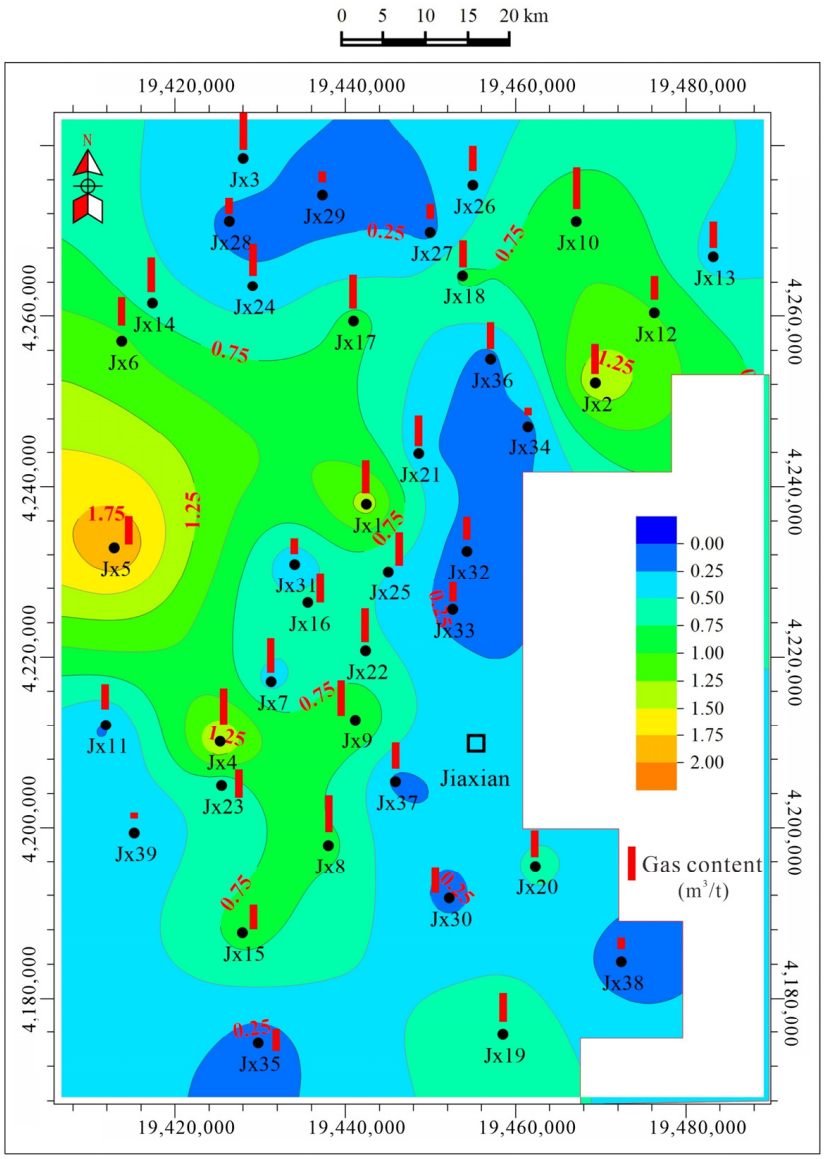


Figure 13. Contour map of failure index of No. 5 coal seam.

From Figure 10f, it could be seen that the CBM content increases with the enlarged damage degree of coal seams. Generally, the coal bodies are easily affected by tectonic activities such as faults, folds, and sliding underground, which might damage the original rock structure. The porosity and permeability of coals would change accordingly. Compared to the small and medium-sized pores, the pores with large diameter in coals are most susceptible to the influence of tectonic action, resulting in a significant increase in pore volume [43]. On the other hand, it has been found that the deformed coals have lower permeability in contrast to the primary coals based on the experimental data on coal permeability at the well site. Therefore, it can be inferred that the large-scale distribution of deformed coals really benefits the enrichment of CBM, thanks to the greatly increased storage space and low permeability. The increase in porosity within the coal seam can expand the gas storage space, and the low permeability of tectonic coal also aids in the preservation of CBM. Therefore, as the degree of coal seam damage increases, the gas content within the coal seam also increases.

5.5. Implications for the Development of DCBM

The study employed a multi-factor calculation method for evaluating coal seam sealing, representing a significant advancement over previous methodologies. This approach

incorporated macro-geological factors such as lithology, the thickness of lithologic layers, and rock breakthrough pressure, alongside micro-geological factors including rock fracture development indices. These considerations collectively contributed to the formulation of a more refined sealing calculation model. Notably, the methodology predominantly relied on logging data, which enabled accurate calculations despite potential constraints in geological data availability. The relationship between sealing properties and coal seam gas content shows that regions characterized by higher sealing properties also exhibited elevated CBM content. This finding not only validates the model's reliability but also underscores its practical applicability. Importantly, these insights hold significant implications for optimizing CBM drilling strategies and enhancing overall CBM production capacity.

Previous studies of various regions have demonstrated the importance of sealing integrity in both the roof and floor regions of coal seams for enhancing CBM preservation and enrichment. In this work of the Jiaxian area, the criticality of roof sealing integrity on gas content emerged as a central theme. CBM enrichment in this area positively correlates with coal thickness, in line with prior research findings. Burial depths within the Jiaxian area typically remain below 2000 m, with high organic matter maturity in coal seams, leading to an overall increase in gas content with depth. Nevertheless, exceeding 1.5% coal maturity reduces porosity and fracture structure, resulting in diminished gas content. Tectonic activities in the Jiaxian locale disrupt coal structures, heightening porosity, reducing permeability, enlarging gas storage capacity, and improving coal seam preservation. Consequently, gas content escalates with the degree of coal seam damage. The coal seam sealing integrity of the Jiaxian area fosters CBM enrichment in tandem with thicker coal deposits. Meanwhile, the elevated temperatures enhance organic matter maturity, reinforcing the upward trend of gas content. The coal seam, influenced by tectonic activities, has favorable storage and preservation conditions, leading to significant CBM enrichment.

The extraction of DCBM in the Jiaxian area faces significant technical challenges. Factors such as significant burial depth, high temperatures, and tectonic faults increase drilling complexity, necessitating strategies such as employing high-temperature-resistant equipment and advanced development technologies to ensure stable operations. Future research on DCBM could focus on two primary areas: Firstly, analyzing the geological characteristics of deep coal reservoirs, including sedimentary environments, coal seam distribution, and related features to enhance understanding of their formation and global distribution in promising CBM-rich areas; and secondly, advancing geophysical exploration and logging technologies. These advancements are crucial for improving CBM resource assessment accuracy, enabling real-time monitoring, optimizing development processes, and mitigating associated risks. In addition to technology, it is accompanied by economic and environmental issues. Increasing extraction depth raises economic costs substantially. Besides, the physical characteristics of deep coal necessitate hydraulic fracturing for enhanced recovery, yet this process can lead to environmental pollution through backflow drainage. Economic and environmental factors require careful consideration following successful DCBM development.

6. Conclusions

(1) A comprehensive evaluation method for the sealing performance of deep coal seam roofs and floors was established using rock mudstone quality, single-layer rock thickness, rock breakthrough pressure, and crack identification index. It is found that the overall sealing of the roof in the Jiaxian area of the Ordos Basin is higher than that of the floor, and it is concentrated in the middle domain. The multifactor roof and floor sealing evaluation model established in this study can reliably evaluate the sealing capacity of the roof and floor using well logs and partial breakthrough pressure experiments in cases where experimental data is insufficient.

(2) Using the roof/floor sealing calculation model, the effect of sealing capacity on gas content was explored. The results indicate that the gas content of the coal seam is jointly controlled by the sealing performance of the roof and floor and increases with

the improvement of their sealing performance. However, the influence of the roof and floor on the gas content is not the same; the roof has a greater impact on the CBM content than the floor.

(3) With the increase in coal seam thickness, the conditions for preserving gas would be boosted; thereby, the gas content in coal seams would also be significantly enhanced. Additionally, with greater burial depth of the coal seam, the high temperatures in the formation lead to increased maturity of the organic matter in the coal, enhancing the gas production capacity of the coal seam. Therefore, the burial depth of the coal seam influences the gas content of the coal seam to a certain extent.

(4) Compared to primary structural coal, tectonic coal exhibits higher porosity due to structural actions that fracture and rearrange the coal seam, while also having numerous microfractures and pores. However, despite the increased porosity, these microfractures and pores are typically irregular and dispersed, resulting in low connectivity and permeability. Consequently, in regions with developed tectonic coal, there is an expansion in reservoir space for gas, which hence promotes CBM preservation. Thus, the extent of coal seam fracturing shows a positive correlation with CBM content to a certain degree.

Author Contributions: Conceptualization, S.X.; data curation, C.Y.; formal analysis, S.X.; funding acquisition, F.Q.; investigation, Z.W.; methodology, S.X.; project administration, Q.L. and F.S.; software, T.Y. and F.Q.; supervision, J.C. and K.Z.; validation, S.X.; writing—original draft, S.X.; writing—review and editing, Q.L. and F.S. All authors have read and agreed to the published version of the manuscript.

Funding: Financial support from National Natural Science Foundation of China (Grant Nos. 42130806, 42202203 and 42372195); Basic Research Ability Enhancement Project for New Teachers (2-9-2023-050).

Data Availability Statement: The data presented in this study are available on request from the corresponding author.

Conflicts of Interest: The authors declare no competing financial interest.

References

1. Qin, Y.; Moore, T.A.; Shen, J.; Yang, Z.; Shen, Y.; Wang, G. Resources and geology of coalbed methane in China: A review. *Int. Geol. Rev.* **2018**, *60*, 777–812. [CrossRef]
2. Li, S.; Qin, Y.; Tang, D.; Shen, J.; Wang, J.; Chen, S. A comprehensive review of deep coalbed methane and recent developments in China. *Int. J. Coal Geol.* **2023**, *279*, 104369. [CrossRef]
3. Yao, Y.; Wang, F.; Liu, D.; Sun, X.; Wang, H. Quantitative characterization of the evolution of in-situ adsorption/free gas in deep coal seams: Insights from NMR fluid detection and geological time simulations. *Int. J. Coal Geol.* **2024**, *285*, 104474. [CrossRef]
4. Guangshan, G.U.; Fengyin, X.U.; Lifang, L.I.; Yidong, C.A.; Wei, Q.I.; Zhaohui, C.H.; Jimei, D.E.; Zhuolun, L.I. Enrichment and accumulation patterns and favorable area evaluation of deep coalbed methane in the Fugu area, Ordos Basin. *Coal Geol. Explor.* **2024**, *52*, 81–91.
5. Li, S.; Tang, D.; Pan, Z.; Xu, H.; Tao, S.; Liu, Y.; Ren, P. Geological conditions of deep coalbed methane in the eastern margin of the Ordos Basin, China: Implications for coalbed methane development. *J. Nat. Gas Sci. Eng.* **2018**, *53*, 394–402. [CrossRef]
6. Yong, L.I.; Lifu, X.U.; Shouren, Z. Gas bearing system difference in deep coal seams and corresponded development strategy. *J. China Coal Soc.* **2023**, *48*, 900–917.
7. Chang, Y.H.; Yao, Y.B.; Wang, L.; Zhang, K. High-Pressure adsorption of supercritical me-thane and carbon dioxide on Coal: Analysis of adsorbed phase density. *Chem. Eng. J.* **2024**, *487*, 150483. [CrossRef]
8. Ren, Q.S.; Zhang, C.; Wu, G.J.; Zhang, H.W.; Gao, S.; Sun, Z.; Gao, Y.R. Hydraulic fracture initiation and propagation in deep coalbed methane reservoirs considering weak plane: CT scan testing. *Gas Sci. Eng.* **2024**, *125*, 205286. [CrossRef]
9. Li, Q.; Li, T.; Cai, Y.; Liu, D.; Li, L.; Ru, Z.; Yin, T. Research progress on hydraulic fracture characteristics and controlling factors of coalbed methane reservoirs. *J. China Coal Soc.* **2023**, *48*, 4443–4460.
10. Wei, Q.; Hu, B.L.; Li, X.Q.; Feng, S.; Xu, H.; Zheng, K.; Liu, H. Implications of geological conditions on gas content and geochemistry of deep coalbed methane reservoirs from the Panji Deep Area in the Huainan Coalfield, China. *J. Nat. Gas Sci. Eng.* **2021**, *85*, 103712. [CrossRef]
11. Zhou, K.; Sun, F.; Yang, C.; Qiu, F.; Wang, Z.; Xu, S.; Chen, J. Evaluation of Deep Coalbed Methane Potential and Prediction of Favorable Areas within the Yulin Area, Ordos Basin, Based on a Mul-ti-Level Fuzzy Comprehensive Evaluation Method. *Processes* **2024**, *12*, 820. [CrossRef]

12. Wei, Q.; Li, X.; Hu, B.; Zhang, X.; Zhang, J.; He, Y.; Zhang, Y.; Zhu, W. Reservoir characteristics and coalbed methane resource evaluation of deep-buried coals: A case study of the No.13-1 coal seam from the Panji Deep Area in Huainan Coalfield, Southern North China. *J. Pet. Sci. Eng.* **2019**, *179*, 867–884. [CrossRef]
13. Xu, F.; Yan, X.; Lin, Z.; Li, S.; Xiong, X.; Yan, D.; Wang, H.; Zhang, S.; Xu, B.; Ma, X. Research progress and development direction of key technologies for efficient coalbed methane development in China. *Coal Geol. Explor.* **2022**, *50*, 1–14.
14. Wang, T.; Zhou, G.X.; Fan, L.Y.; Zhong, C.H. Full-Scale Pore and Microfracture Characterization of Deep Coal Reservoirs: A Case Study of the Benxi Formation Coal in the Daning-Jixian Block, China. *Int. J. Energy Res.* **2024**, *2024*, 5772264. [CrossRef]
15. Chen, B.; Li, S.; Tang, D.; Pu, Y.; Zhong, G. Evaluation of recoverable potential of deep coalbed methane in the Linxing Block, Eastern Margin of the Ordos Basin. *Sci. Rep.* **2024**, *14*, 9192. [CrossRef] [PubMed]
16. Chen, G.; Hu, Z.Q. Discussion on the model of enrichment and high yield of deep coalbed methane in Yanchuannan area at South eastern Ordos Basin. *J. China Coal Soc.* **2018**, *43*, 1572–1579.
17. Zhao, B.; Liu, D.M.; Cai, Y.D.; Zhao, Z.; Sun, F.R. Geological Control Mechanism of Coalbed Methane Gas Component Evolution Characteristics in the Daning-Jixian Area, Ordos Basin, China. *Energy Fuels* **2023**, *37*, 19639–19652. [CrossRef]
18. Chen, H.D.; Li, J.; Zhang, C.G.; Cheng, L.X. Discussion of sedimentary environment and its geological enlightenment of Shanxi Formation in Ordos Basin. *Acta Petrol. Sin.* **2011**, *27*, 2213–2229.
19. Bian, C.S.; Zhao, W.Z.; Wang, H.J.; Chen, Z.Y.; Wang, Z.C.; Liu, G.D.; Zhao, C.Y.; Wang, Y.P.; Xu, Z.H.; Li, Y.X.; et al. Contribution of moderate overall coal-bearing basin uplift to tight sand gas accumulation: Case study of the Xujiahe Formation in the Sichuan Basin and the Upper Paleozoic in the Ordos Basin, China. *Pet. Sci.* **2015**, *12*, 218–231. [CrossRef]
20. Zhai, Y.; He, D.; Kai, B. Tectono-depositional environment and prototype basin evolution in the Ordos Ba-sin during the Early Permian. *Earth Sci. Front.* **2023**, *30*, 139–153.
21. Yang, W.; Wang, F. Sedimentary environments and sandbody distribution in member 2 of Permian Shanxi formation in mid-eastern Ordos Basin. *Sci. Technol. Rev.* **2016**, *34*, 110–115.
22. Wang, Z.; Cai, Y.; Liu, D.; Qiu, F.; Sun, F.; Zhou, Y. Intelligent classification of coal structure using multi-nomial logistic regression, random forest and fully connected neural network with multisource geophysical logging data. *Int. J. Coal Geol.* **2023**, *268*, 104208. [CrossRef]
23. Kang, J.; Fu, X.; Shen, J.; Liang, S.; Chen, H.; Shang, F. Characterization of coal structure of high-thickness coal reservoir using geophysical logging: A case study in Southern Junggar Basin, **njiang, Northwest China. *Nat. Resour. Res.* **2022**, *31*, 929–951. [CrossRef]
24. Tian, F.C.; Liang, Y.T.; Wang, D.M.; Jin, K. Effects of caprock sealing capacities on coalbed methane preservation: Experimental investigation and case study. *J. Cent. South Univ.* **2019**, *26*, 925–937. [CrossRef]
25. Feng, H. Cap rock influence on coalbed gas enrichment in Qinshui Basin. *Nat. Gas Ind.* **2005**, *25*, 34.
26. Busch, A.; Alles, S.; Gensterblum, Y.; Prinz, D.; Dewhurst, D.N.; Raven, M.D.; Stanjek, H.; Krooss, B.M. Carbon dioxide storage potential of shales. *Int. J. Greenh. Gas Control.* **2008**, *2*, 297–308. [CrossRef]
27. Shi, H.; Zhou, J.; Wang, L.; Sun, M.; Xiang, Y. Logging interpreation and regional prediction of mudstone breakthrough pressures in the upper paleozic, South Ordos Basin. *Geo-Phys. Geochem. Explor.* **2014**, *38*, 63–70.
28. Ellsworth, W.L. Injection-induced earthquakes. *Science* **2013**, *341*, 1225942. [CrossRef] [PubMed]
29. Aghli, G.; Soleimani, B.; Moussavi-Harami, R.; Mohammadian, R. Fractured zones detection using conventional petrophysical logs by differentiation method and its correlation with image logs. *J. Pet. Sci. Eng.* **2016**, *142*, 152–162. [CrossRef]
30. Ge, X.M.; Fan, Y.R.; Zhu, X.J.; Deng, S.G.; Wang, Y. A Method to Differentiate Degree of Volcanic Reservoir Fracture Development Using Conventional Well Logging Data-An Application of Kernel Principal Component Analysis (KPCA) and Multifractal Detrended Fluctuation Analysis (MFDFA). *IEEE J. Sel. Top. Appl. Earth Obs. Remote Sens.* **2014**, *7*, 4972–4978. [CrossRef]
31. Dong, S.; Zeng, L.; Lyu, W.; Xu, C.; Liu, J.; Mao, Z.; Tian, H.; Sun, F. Fracture identification by semi-supervised learning using conventional logs in tight sandstones of Ordos Basin, China. *J. Nat. Gas Sci. Eng.* **2020**, *76*, 103131. [CrossRef]
32. Lyu, W.Y.; Zeng, L.B.; Liu, Z.Q.; Liu, G.; Zu, K. Fracture responses of conventional logs in tight-oil sandstones: A case study of the Upper Triassic Yanchang Formation in southwest Ordos Basin, China. *Aapg Bull.* **2016**, *100*, 1399–1417. [CrossRef]
33. Li, Z.; Fan, C.; Sun, B.; Han, X.; Hui, X.; Deng, X.; Wang, A.; Wang, G. Characteristics, logging identification and major controlling factors of bedding-parallel fractures in tight sandstones. *Geoenergy Sci. Eng.* **2023**, *228*, 211956. [CrossRef]
34. Guo, D.L.; Zhu, K.; Wang, L.; Li, J.; Xu, J. A new methodology for identification of potential pay zones from well logs: Intelligent system establishment and application in the Eastern Junggar Basin, China. *Pet. Sci.* **2014**, *11*, 258–264. [CrossRef]
35. Tóth, E.; Hrabovszki, E.; Tóth, T.M. Using geophysical log data to predict the fracture density in a claystone host rock for storing high-level nuclear waste. *Acta Geod. Et Geophys.* **2023**, *58*, 35–51. [CrossRef]
36. Ambati, V.; Sharma, S.; Babu, M.N.; Nair, R.R. Laboratory measurements of ultrasonic wave velocities of rock samples and their relation to log data: A case study from Mumbai offshore. *J. Earth Syst. Sci.* **2021**, *130*, 18. [CrossRef]
37. Aghli, G.; Aminshahidy, B. Evaluation of Open Fractures-Sonic Velocity Relation in Fractured Carbonate Reservoirs. *SPE J.* **2022**, *27*, 1905–1914. [CrossRef]
38. Yue, C.W.; Yue, X.P. Simulation of acoustic wave propagation in a borehole sur-rounded by cracked media using a finite difference method based on Hudson's ap-proach. *J. Geophys. Eng.* **2017**, *14*, 633–640. [CrossRef]
39. Li-Han, Z.; Guang-Sheng, Z. Improvement and Application of the Methods of Gas Reservoir Cap Sealing Ability. *Acta Sedimentol. Sin.* **2010**, *28*, 388–394.

40. Liu, D.; Jia, Q.; Cai, Y.; Gao, C.; Qiu, F.; Zhao, Z.; Chen, S. A new insight into coalbed methane occurrence and ac-cumulation in the Qinshui Basin, China. *Gondwana Res.* **2022**, *111*, 280–297. [CrossRef]
41. Liu, D.; Yao, Y.; Wang, H. Structural compartmentalization and its relationships with gas accumulation and gas production in the Zhengzhuang Field, southern Qinshui Basin. *Int. J. Coal Geol.* **2022**, *259*, 104055. [CrossRef]
42. Cai, Y.; Liu, D.; Yao, Y.; Li, J.; Qiu, Y. Geological controls on prediction of coalbed methane of No. 3 coal seam in Southern Qinshui Basin, North China. *Int. J. Coal Geol.* **2011**, *88*, 101–112. [CrossRef]
43. Cheng, Y.; Pan, Z. Reservoir properties of Chinese tectonic coal: A review. *Fuel* **2020**, *260*, 116350. [CrossRef]

Disclaimer/Publisher's Note: The statements, opinions and data contained in all publications are solely those of the individual author(s) and contributor(s) and not of MDPI and/or the editor(s). MDPI and/or the editor(s) disclaim responsibility for any injury to people or property resulting from any ideas, methods, instructions or products referred to in the content.